AFM Microcantilever With a Collocated AlN Sensor-Actuator Pair: Enabling Efficient *Q*-Control for Dynamic Imaging

Mohammad Mahdavi, *Member, IEEE*, Nastaran Nikooienejad, and S. O. Reza Moheimani, *Fellow, IEEE*

***Abstract*— This manuscript presents a novel microcantilever with an embedded piezoelectric sensor-actuator pair for dynamic atomic force microscopy (AFM). The transducer pair is constructed from a two-layered AlN stack. Stacking the piezoelectric transducers in this manner leads to a minimal feedthrough from actuation to sense electrode, granting a high dynamic range frequency response for dynamic mode AFM. The cantilever's design allows for dual mode operation at 1st and 2nd resonance modes. High resolution tapping mode imaging results are reported, while the cantilever is operated at these modes. A feedback control loop is used to modify quality factor of the 1st mode of the cantilever, using a positive position feedback (PPF) controller. A faster response time is achieved by reducing the *Q*-factor, enabling the cantilever to track the topography at a higher scan rate. Results of bimodal AFM imaging are reported, using amplitude changes of the 1st mode for surface topography, while material properties are encoded in phase changes of the 2nd mode.**

[2020-0096]

***Index Terms*— Atomic force microscopy (AFM), tapping mode AFM, active microcantilever, microelectromechanical system (MEMS), dynamic range, *Q*-control.**

I. Introduction

DYNAMIC mode atomic force microscopy (AFM) is of much interest in studying topography and material properties of soft samples. Due to the intermittent tip-sample contact, lateral forces that complicate contact-mode AFM operations are eliminated enabling non-invasive surface microscopy with a minimum tip wear [1]. Dynamic-mode AFM can reveal further information on mechanical properties of the surface such as its elastic modulus and viscosity, which are not available in contact-mode imaging. These advantages of dynamic imaging can further be extended with multifrequency/multimode AFM methods.

In a conventional AFM setup, a passive Si microcantilever actuated by a piezoelectric base shaker, is forced to vibrate near its resonance frequency, while its amplitude of oscillation is measured using the optical beam deflection (OBD) method. This actuation/sensing arrangement makes it difficult to control the dynamics of the microcantilever, and to reduce its dimensions for on-chip and array realization of AFMs. This has led to a significant interest in microfabricated cantilevers with on-chip sensors and actuators. In particular, if the sensor and actuator are collocated, it is possible to design and implement highly efficient feedback controllers to arbitrarily change the quality factor of the cantilever. This is known as *Q*-control [2].

Piezoelectric transduction has been among the most practical approaches for self-actuation/sensing of the cantilever vibration. However, electrical feedthrough from actuation signal to readout has been a persisting problem associated with this approach, limiting the dynamic range (DR) and signal to noise ratio (SNR) of the device. The feedthrough signal dominates the resonant induced piezoelectric effect, thus the sensor cannot capture the dynamics of the cantilever near the resonance. Off-chip feedthrough cancellation methods are usually employed to subtract the feedthrough path and increase the DR [3]. However, additional electronics for mimicking and subtracting the feedthrough in such approaches lead to higher noise baselines worsening the SNR. Also, these methods have shown to be working within a limited frequency band, thus require further tuning at other frequency ranges in multi-frequency AFMs. Two arrangements for on-chip feedthrough cancellation, based on differential sensing and pseudo actuation concepts, were previously reported by our group [4]. These methods lead to higher DR and SNR, but still cannot achieve the same level of performance as the OBD method.

We recently reported a new type of piezoelectric microcantilevers with self-actuation and sensing capabilities. A two-layer stack piezoelectric transducer enables three ports: actuation, ground and sense. The feedthrough capacitive path between actuation and sense ports is minimized to achieve a high dynamic range operation at the 1^{st} flexural resonance mode. In addition, collocation of the sensor-actuator pair on the cantilever results in negative-imaginary frequency responses, guaranteeing closed-loop stability when used in a feedback loop in conjunction with a strictly negative-imaginary controller.

In present work, the mechanical structure of the cantilever is changed to enable dual mode operation at the 1^{st} and 2^{nd} resonance modes; located at 52 kHz and 329 kHz respectively. The anchoring point of the device layer to the handle substrate

Manuscript received April 27, 2020; revised July 19, 2020; accepted July 20, 2020. Date of publication July 31, 2020; date of current version October 7, 2020. This work was supported by the U.S. Department of Energy's Office of Energy Efficiency and Renewable Energy (EERE) under the Advanced Manufacturing Office under Grant DE-EE0008322. Subject Editor M. Rais-Zadeh. *(Corresponding author: Reza Moheimani.)*

The authors are with the Erik Jonsson School of Engineering and Computer Science, The University of Texas at Dallas, Richardson, TX 75080 USA (e-mail: reza.moheimani@utdallas.edu; reza.moheimani@utdallas.edu).

Color versions of one or more of the figures in this article are available online at http://ieeexplore.ieee.org.

Digital Object Identifier 10.1109/JMEMS.2020.3011826

is moved toward the substrate. Consequentlly, mode shapes of the cantilever and piezoelectric sensor dynamics are changed in favor of operating the probe in dual mode AFM. Operating the cantilever at its 2^{nd} mode, i.e. at a higher frequency, provides adequate bandwidth for fast scanning. Furthermore, reducing Q of the 1^{st} mode facilitates cantilever operation at this mode. Modulated-demodulated technique is utilized for implementation of a PPF controller. This realization with wideband lock-in amplifiers enables flexibile tuning of controller parameters on the fly and is highly suitable for rapid prototyping applications.

In section II of this report, we briefly describe the design criteria of the microcantilever and present electromechanical characterization results. Section III explains the Q-control design and closed-loop system characterization. In section IV, results of tapping mode AFM imaging at both modes are demonstrated, and response times of operation at the 1^{st} mode with and without Q-control are compared accordingly. Also, we perform bimodal AFM imaging to capture topographic and phase image of a polymer blend sample. The phase changes of the 2^{nd} mode are recorded, when the amplitude changes of the 1^{st} mode follow the surface topography.

II. Electromechanical Design and Characterization

A. Microcantilevers Design

Active microcantilevers with piezoelectric actuation and sensing have emerged as good candidates to replace OBD method in dynamic AFM. However, microfabrication of closely spaced piezoelectric transducers on microcantilevers leads to electrical parasitics which worsens the dynamic range [4]. Separation of actuation transducer from the sense transducer is a common approach to minimize capacitive feedthrough path from actuation to sense electrode [5], [6]. However, actual realization of such active microcantilevers requires a large surface area to provide enough space for both actuation and sense transducers, and maximize sensor electrode dimensions for collection of vibration induced charges. As an alternative, one can stack the transducers on top of each other to allow optimal use of available surface area on the cantilever for the sense electrode, especially in case of small cantilevers operating at higher frequencies [7].

The proposed cantilever is made of a 3 μm thick Si layer with dimensions of 345 μm and 100 μm in length and width, respectively; see SEM image of Fig. 1(a). A two-layer piezoelectric stack transducer is microfabricated on top of the microcantilever as a collocated actuation/sensing pair. The top AlN piezoelectric transducer, in-between top Al electrode and middle Mo electrode is used to stimulate the cantilever into vibration. The bottom transducer, which is sandwiched between middle and bottom Mo electrodes, is used for measuring vibration-induced charges. Figure 1(b) illustrates the cross-sectional view of the cantilever showing the constructing materials and electrical connections for excitation and readout. Further information on microfabrication of the microcantilever is reported in [7].

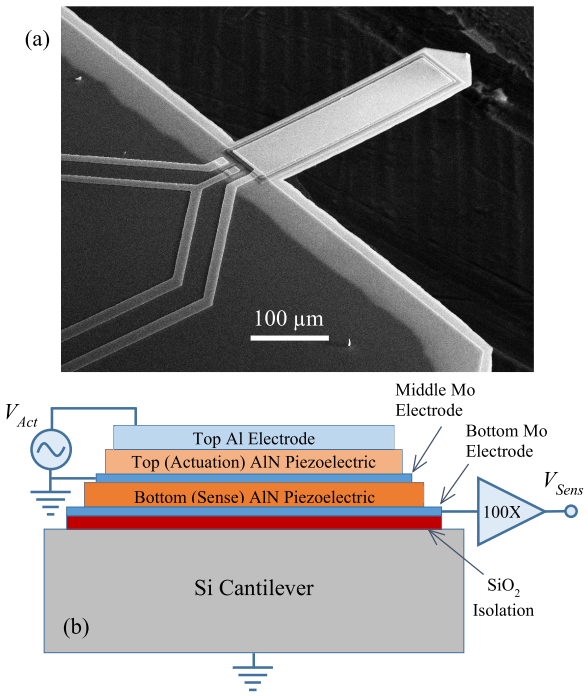

Fig. 1. (a) SEM image of the microfabricated Si cantilever with a collocated actuator-sensor pair. (b) Cross-sectional view of the cantilever showing the constructing materials of the cantilever and the actuator-sensor stack transducers.

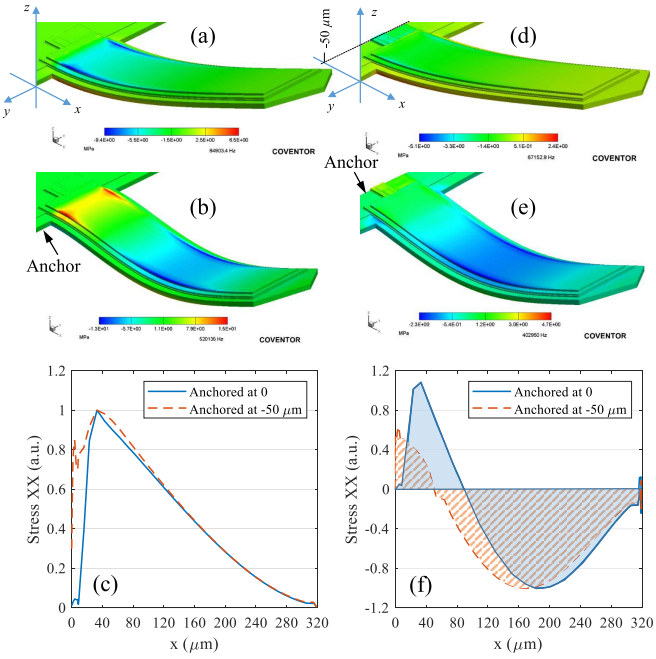

Fig. 2. Mode shapes of the first and second modes of the cantilevers: (a) and (b) anchored at 0 μm and (d) and (e) anchored at -50 μm. The color code maps stress along X axis (StressXX). (c) and (f) are stress profiles of the first and second resonance modes along X axis on the piezoelectric sensor. The profile is normalized to provide a fair comparison of two cantilevers.

1) Mechanical Design: Generally, cantilevers following Euler-Bernolli beam theory show a dominant first flexural resonance mode, and the amplitude of vibration at the second mode is more than an order of magnitude smaller. Figures 2(a) and (b) show mode shapes of the 1^{st} and 2^{nd} resonance modes

of such a cantilever. Consdiering reasonable damping in air at these modes, one expects amplitude ratio of $A_2/A_1 \approx 0.05$ excited with the same voltage amplitude.

A piezoelectric transducer covers the cantilever surface to measure cantilever vibrations. The color code on mode shapes in Fig. 2 maps mechanical stress along X axis of the cantilever (stressXX). The stress corresponds to the cantilever bendig or the second derivative of the cantilever transverse vibration. As the stress profile of the 1^{st} mode suggests, the piezoelectric sensor experiences the maximum stress at the anchoring point with zero displacement and a zero stress at the free vibrating end of the cantilever (see blue color code in Fig. 2(a)). The output charge of the piezoelectric sensor is a weighted average of the surface stress. In other words, the ouput charge of the sensor at the 1^{st} mode is an integration of stress induced charges on the piezoelectric sensor and is proportional to the area under the bule curve (normalized stress profile) in Fig. 2(c). For the second mode, there is a positive and a negative maximum stress along X axis, which are painted respectively in red and blue color codes in the mode shape of Fig. 2(b). Similarly, the ouput charge of the second mode is proportional to the area under the bule curve of the Fig. 2(f). Thus, almost half of the charges induced in the piezoelectric sensor on negative stress area are cancelled out with charges on the area under positive stress. The deflection sensing gain at the second mode is consequently smaller.

The cantilevers reported in [7] obey such behavior and are highly suitable for operation in the 1^{st} mode. However, proper modifications are required to accomodate dual mode operation. A change is introduced to the mechanical structure of the cantilever to satisfy this requirement. The anchoring point of the device layer to the handle layer is placed with a spacing of 50 μm from the spot where the cantilever is attached to the device layer. This feature is clear in the gray area between cantilever and the substrate in Fig. 1(a).

Mode shapes corresponding to the 1^{st} and 2^{nd} modes for this modified cantilever are shown in Fig. 2(d) and (e) respectively. Although the mode shape at the 1^{st} mode is slightly changed, the piezoelectric sensor expriences a similar stress profile to the cantilever reported in [7]. The stress profile of the modified cantilever is shown with dashed orange line in Fig. 2(c) in comparison with the stress profile of the previous cantilever. Due to this modification, the actuation gain at this mode is smaller than the privous case. However, a considerable change is observed on the mode shape of the 2^{nd} mode. The area under positive stress is now narrower with a less stress intensity, while the area under negative stress is expanded along the sensor. This behavior is depicted in stress profile of dashed orange line in Fig. 2(f). The portion of cancelled charges of the area under negative stress by positive stress is relatively less than previous case (see shaded orange areas compared with blue areas under curves). This leads to a relatively higher displacement sensitivity at the 2^{nd} mode. Consequently, ratio of vibration amplitude of the 2^{nd} mode to the 1^{st} mode is more than previous cantilever. The increase in actuation and sense gains at 2^{nd} mode relative to the 1^{st} mode makes this modified cantilever a better candidate for dual mode operation.

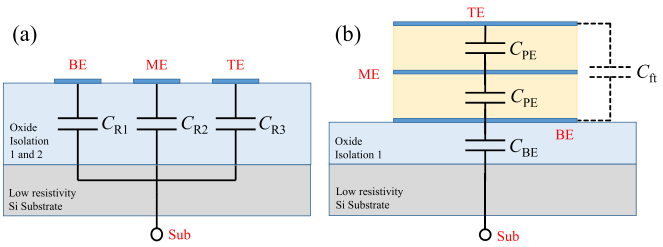

Fig. 3. Dielectric capacitances: (a) between signal routings and the substrate and (b) between electrodes and the substrate.

2) Electrical Feedthrough: Despite differences outlined above, feedthrough mitigation is still equally effective. The feedthrough capacitance emerges from two sources: electrical routings on the probe substrate and piezoelectric layer dielectric capacitances. These capacitances are shown in the capacitive model of Fig. 3, in which, C_Rs represent capacitances from each of Al routings to the conductive substrate, due to the oxide isolation layer, C_{PE} between top/bottom electrodes to the middle electrode on the cantilever through AlN piezoelectric layers, and C_{BE} between the bottom electrode and the substrate. Ideally, these capacitances are eliminated by connecting the middle electrode and the substrate to the ground, and there is no capacitive path from actuation (TE) to sense electrode (BE). In practice, a small feedthrough capacitance exists between the actuation and sense electrodes, which is significantly smaller than dielectric capacitances. The effect of this small capacitance shows up in higher frequency responses of the cantilever, which is beyond the desired frequency range.

B. Characterization

The modal responses of the cantilever are characterized with a lock-in amplifier (LIA) and the laser Doppler vibrometer (LDV). The cantilever is stimulated into vibration by applying a sine voltage to the top electrode, while the sense electrode is fed to a readout amplifier circuit with a voltage gain of 100X. The output of the readout circuit is fed back to the LIA as an input. The frequency response functions (FRFs) from the actuation voltage to the amplified sense signal are collected near the 1^{st} and 2^{nd} resonance modes. The magnitude and phase of the FRFs are plotted with solid blue lines in Fig. 4(a) and (b).

To characterize vibration of the cantilever near these two modes by LDV, the cantilever is actuated by a sine voltage delivered to the top electrode, while the laser beam is pointing at the tip of the cantilever. The FRFs obtained with this method are plotted in the same Fig. 4(a) and (b) with dashed red lines for comparison. It is clear that the piezoelectric displacement sensor response follows the dynamics of the cantilever near resonances with a high dynamic range. Vibration induced charges on the sensor electrode dominate the feedthrough charges, and therefore high dynamic ranges are achieved.

A summary of performance of the cantilever based on measurements obtained from piezoelectric displacement sensor at these modes is presented in Table I. The SNRs are measured while the cantilever is excited with a 100 mV actuation voltage. Owing to comparable DRs, Qs and SNRs at both modes,

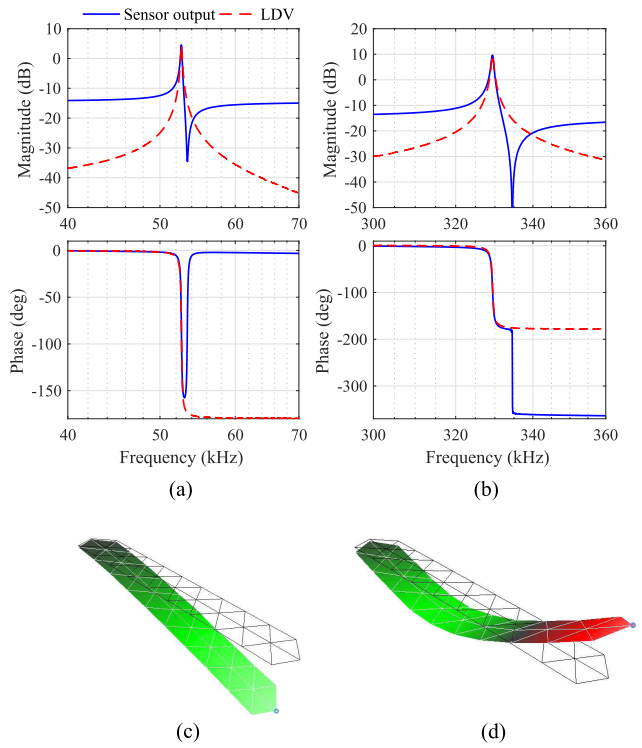

Fig. 4. Frequency responses of the microcantilever measured by the piezoelectric sensor (blue line) and laser Doppler vibrometer (LDV): (a) 1^{st} and (b) 2^{nd} resonance modes. Mode shapes of the (c) 1^{st} and (d) 2^{nd} resonance modes.

TABLE I
SUMMARY OF MODAL RESPONSES OF THE CANTILEVER

Resonance Mode	f_0 (kHz)	Actuation Gain (nm/mV)	Deflection Sensitivity (mV/nm)	Q	DR (dB)	SNR $(dB/\sqrt{Hz})$
1^{st}	52.673	3.124	1.466	312	18.67	106.49
2^{nd}	329.404	1.478	6.522	561	23.16	109.4

the cantilever is an appropriate candidate for multifrequency dynamic mode AFM imaging.

III. Q-CONTROL OF THE MEMS CANTILEVER

The inherent high Q of the MEMS microcantilever leads to a narrow bandwidth, which appears in its transient response when tracking sharp features on the sample. In this respect, actively damping the cantilever's resonance increases the tracking bandwidth, which in turn allows for larger feedback gains in z-axis feedback controller and a faster response time [2]. A common approach to attenuate a resonant mode is to use a positive position feedback (PPF) controller. This controller functions similar to a differentiator in the vicinity of the cantilever resonance resulting in velocity feedback despite the displacement-like measurement being available to the controller. Hence, the quality factor of the cantilever can be modified by tuning the gain of the controller. When compared to other Q-control techniques, due to a second order compensator with a low-pass behavior, the PPF controller

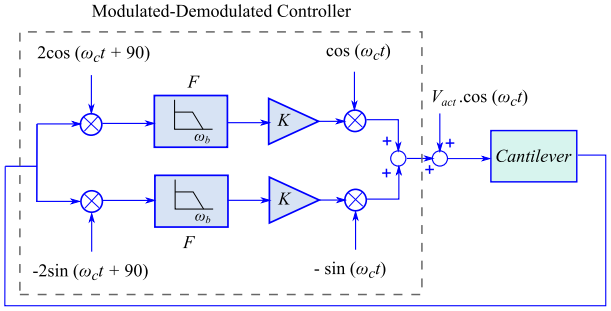

Fig. 5. Schematic of involvement of the microcantilever within a control loop for active Q-control using modulated-demodulated technique.

provides rapid roll-off to prevent spill-over into higher modes. Moreover, according to the negative imaginary (NI) theory, positive feedback interconnection of the PPF controller with a cantilever, as a negative imaginary system, guarantees closed-loop stability of the system in presence of unmodeled cantilever dynamics [6], [8].

Direct implementation of a high-bandwidth controller to dampen the resonant modes introduces a large phase lag due to the significant time delay at high frequency, which can destabilize the control loop system and degrade its performance. Alternatively, since the resonant modes have a band-pass nature, a low-bandwidth controller can be synthesized to augment the damping of the 1^{st} resonance using the modulated-demodulated technique [9].

As illustrated in Fig. 5, each branch of the modulated controller consists of a demodulator, a baseband controller, and a modulator. The modulator and demodulator operate in quadrature/in-phase (QI) structure. The demodulator translates the sensor output to baseband from resonance, while the modulator converts the control signal back to resonance passband. The carrier frequency (ω_c) is selected equivalent to the cantilever's resonance frequency to estimate the velocity at resonance.

Here, we design and implement a PPF controller using the modulated-demodulated technique; see [10] for further detail. In this configuration, the baseband controller involves a variable gain (K) and a first-order low-pass filter (F). Accordingly, the equivalent LTI system is a PPF controller [10] as

$$C_{PPF}(s) = \frac{2K\omega_b\omega_c}{(s+\omega_b)^2+\omega_c^2} \tag{1}$$

where ω_c is the carrier frequency and ω_b is the cut-off frequency of the low-pass filter. To effectively reduce the quality factor to a desired value, the controller parameters are extracted by solving a constrained optimization problem considering the DC gain condition in NI theory [10].

This technique was previously utilized for controlling Q-factor of flexible structures equipped with piezoelectric actuators and sensors [9] and an AFM microcantilever with a single piezoelectric actuator [10]. In contrast to these studies, here we demonstrate how such a modulated-demodulated control system can be realized with off-the-shelf equipments.

To implement the modulated-demodulated controller, we use HF2LI lock-in amplifier and Analog Devices

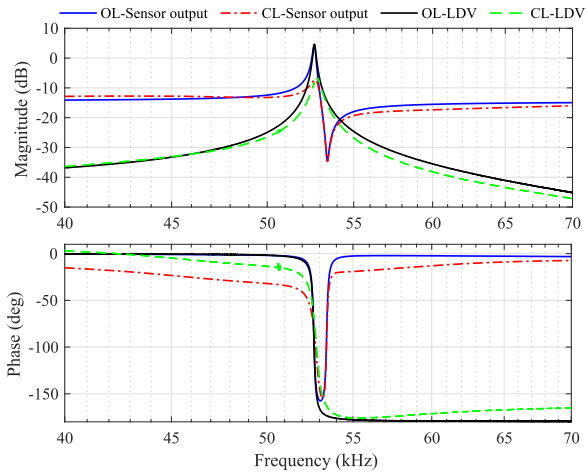

Fig. 6. Experimental frequency responses of the microcantilever with and without *Q*-control measured by the piezoelectric sensor and LDV.

AD831 low-distortion mixers as the demodulator and modulator, respectively. The detailed interconnections between different parts of the controller are shown in Fig. 7(d). In the experimental setup, LIA-2 demodulates the sensor output and generates the in-phase (I), and quadrature (Q) carrier sources for the local oscillators (LOs). The LO-I, LO-Q, and in-phase and quadrature components of the baseband signals, denoted by X and Y, are fed into the mixers. Then, the mixers output, IF-I and IF-Q, are combined and filtered with a SR560 low-noise voltage preamplifier. As depicted in Fig. 7, LIA-1 is used for excitation and reading out the sensor output, while combining the controller output with actuation signal for active *Q*-control. The variable gain K and the low-pass filter's cut-off frequency f_b can be adjusted within LIA-2 to obtain the desired Q. The proposed experimental setup is straightforward to implement, which provides a flexible, wide dynamic range and low-noise configuration in comparison to a custom-designed circuitry.

Here, we reduce the Q to 109 to augment the damping of the resonance at the 1^{st} mode and achieve an acceptable dynamic range. The desired Q is obtained by tuning controller parameters to $K = 1.5$ and $f_b = 8.7$ kHz. The experimental FRF from actuation to sensor output with and without *Q*-control are compared in Fig. 6. Similarly, frequency responses of the tip displacement in open loop and closed loop acquired with LDV are compared with the piezoelectric sensor response. We observe that the quality factor is reduced effectively which is translated to larger z-axis bandwidth for tapping-mode AFM.

IV. AFM Imaging

We perform tapping mode AFM imaging at the 1^{st} and 2^{nd} modes to capture the topographic image of a calibration grating with step heights of 110 nm and a period of 3 μm. Efficiency of the implemented *Q*-control method is demostrated while tracking downward edges of the sample. To study the effect of elastic moduli on the phase of the 2^{nd} mode, we also conduct bimodal AFM imaging on a Bruker PS-LDPE sample. As shown in Fig. 8(b) and (c), the microcantilever is connected to a voltage amplifier circuit and mounted on a custom-designed cantilever holder to integrate with a AFMWorkshop TT-AFM.

A. Tapping Mode

Slow transient response of the cantilever appears as the scan rate becomes faster in high-speed tapping mode imaging. Therefore, imaing experiments are conducted at the fastest possible scan rate enabled by the commmercial AFM used here which is 60 μm/s. The cantilever features a high Q of 312, when operating at the 1^{st} mode, which is translated to a narrow z-axis bandwidth of 170 Hz for tapping mode AFM. Such a narrow bandwidth slows down the transient response of the closed-loop imaging system, leading to parachuting effect while capturing step-like features on the topography shown in Fig. 8(a). Consequently, *Q*-controlled microcantilever operating at the 1^{st} mode is used for capturing the same feature; see Fig. 8(b). With lower Q and hence a wider bandwidth, the cantilever exhibits a faster response time; see the height profile comparison depicted in Fig. 8(c).

To ensure the stability of the closed-loop system and achieve high-performance tracking, the loop gain must be small enough at resonance. However, the high quality factor of the microcantilever reduces the gain margin and may cause instability at high-speed scanning. Applying the *Q*-control reduces the quality factor of the cantilever and decreases the gain at resonance, accordingly. This provides enough gain margin and allows for an increase in the gain of tracking controller, which is a proportional-integral (PI) controller, here. As Fig. 8(d) illustrates, by further increasing the PI gain, a significant ringing appears in tracking response of the microcantilever without *Q*-control.

Although cantilever's 2^{nd} mode quality factor is approximately twice that at the 1^{st} mode, higher resonance frequency of cantilever at this mode results in a faster response even without the *Q*-control. Fig. 9 depicts the topography of the same features when the cantilever is operating at the 2^{nd} mode without *Q*-control.

B. Bimodal Imaging: Phase Imaging

In a bimodal AFM setup of this experiment, the cantilever is excited to vibrate at the 1^{st} and 2^{nd} modes simultaneously. Changes in vibration amplitude of the 1^{st} mode, A_1, are used to track the topography of the surface i.e. regular tapping mode AFM, while changes in phase of the 2^{nd} mode reflects changes in elastic modulus of the surface [11]. The relationship between the second mode parameters and the gradient of the interaction force at distance d from the sample is ($A_{02} \ll A_{01}$)

$$\frac{dF_{ts}}{dz}(d) \propto \frac{k_2 A_{02}}{Q_2 A_2} \cos\phi_2 \tag{2}$$

in which k_2, Q_2, A_{02}, A_2 are dynamic stiffness, quality factor, free air vibration amplitude and contact amplitude of the 2^{nd} mode. Furthermore, based on Hertz contact mechanics model,

$$\frac{dF_{ts}}{dz} = 2E_{eff}a \tag{3}$$

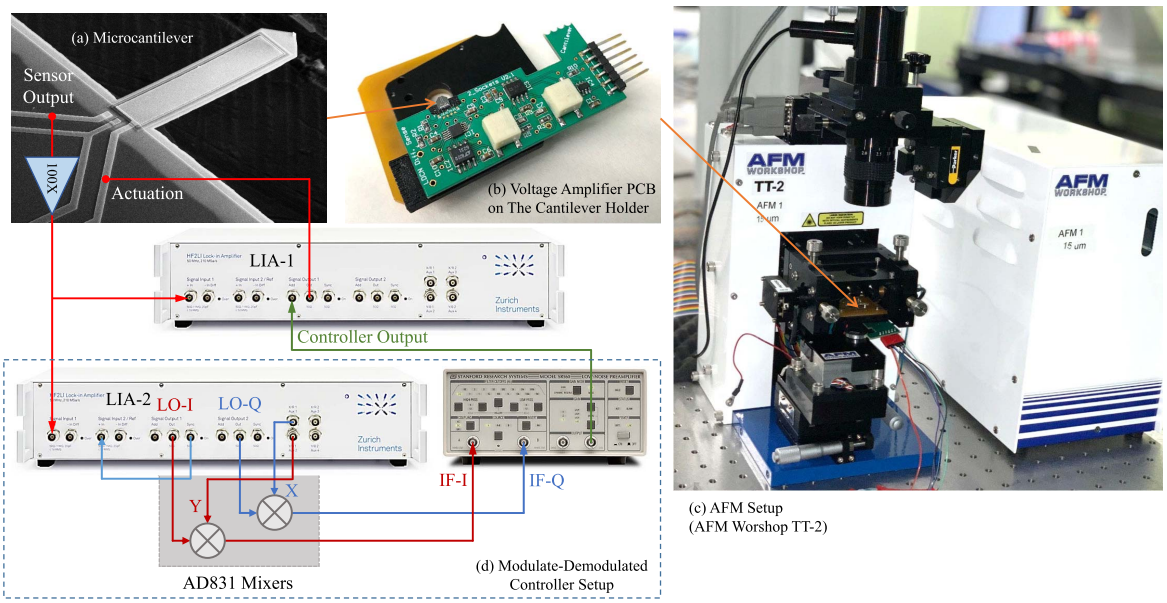

Fig. 7. The complete AFM imaging setup including: (a) The active microcantiever with a sensor-actuator transducer pair, (b) The cantilever mounted on the volage amplifier PCB board (The PCB board is loaded on a custom designed cantilever holder), (c) TT-2 AFM setup with the cantilever holder, and (d) Modulated-demodulated controller setup for the active Q-control of the cantilever. LIA-1 is used for feeding the actuation signal to the cantilever and demodulating the sensor output.

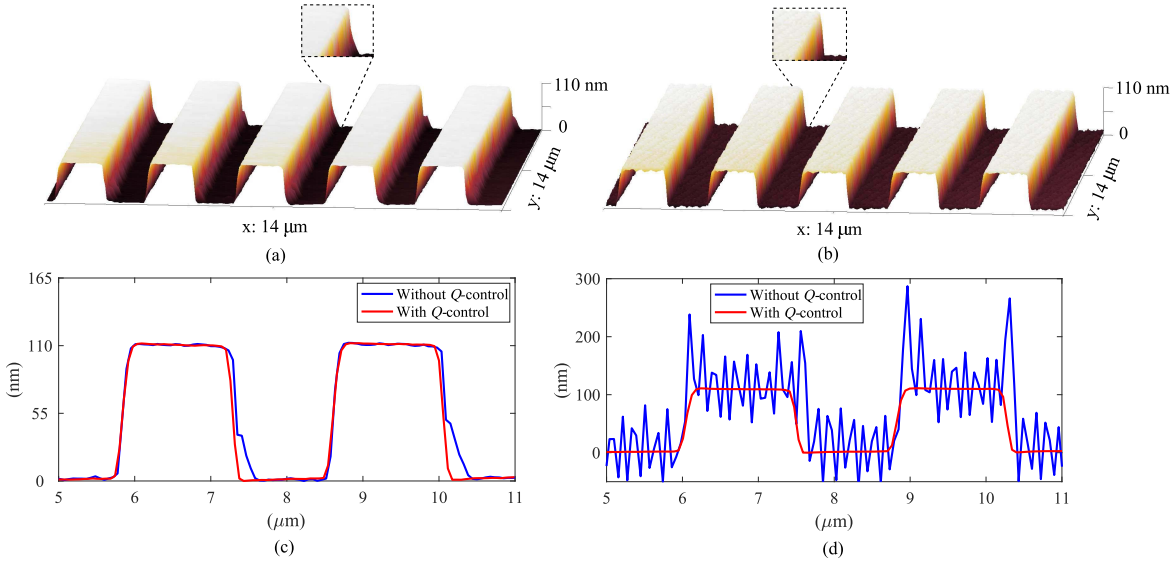

Fig. 8. AFM images of a calibration grating at the 1^{st} mode (a) without Q-control (b) with Q-control. (c) Height profile of the calibration grating with and without Q-control. (d) Height profile of the calibration grating after an increase in feedback gain.

where a and E_{eff} are the effective contact radius and elastic modulus [11]. Here, the sample is a blend of Polystyrene (PS) and low density Polyolefin Elastomer (LDPE) with elastic moduli of approximately 2 GPa and 0.1 GPa, respectively. According to (3), higher phase shifts are expected on PS regions compared to PE.

The first and second mode free air vibration amplitudes are set to $A_{01} = 625$ nm and $A_{02} = 100$ nm. The set amplitude of $A_1 = 343$ nm is selected for the 1^{st} tapping mode which is translated to %55 of the free air amplitude. Qs are reported in Table I, and spring constants are calculated as 15 N/m and 403 N/m approximately. The results of bimodal imaging are illustrated in Fig. 10. Figure 10(a) and (b) show 2D and 3D profiles of topographies of the sample in an area of $5 \times 5\ \mu m^2$ captured by the 1^{st} mode. The PS regions are distinguished as hill-liked features in the 3D topographic profile. Also, a 2D image of phase difference of the second mode is shown in Fig. 10(c); distinguished by dark regions of PS vs. bright regions of LDPE [12]. It should be noted, that the phase difference is calculated by substracting the phase ϕ_2 from 90 degree phase at resonance. Figure 10(d) shows phase contrast distribution over the imaging area. Thus, a cantilever with these bimodal imaging parameters is capable of distinguishing these two different polymer phases with a phase contrast of $\Delta\phi_2 \approx 50$ degree.

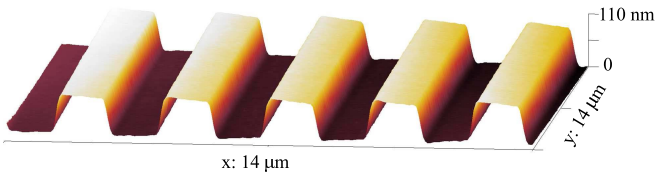

Fig. 9. AFM image of a calibration grating at the 2^{nd} mode without *Q*-control.

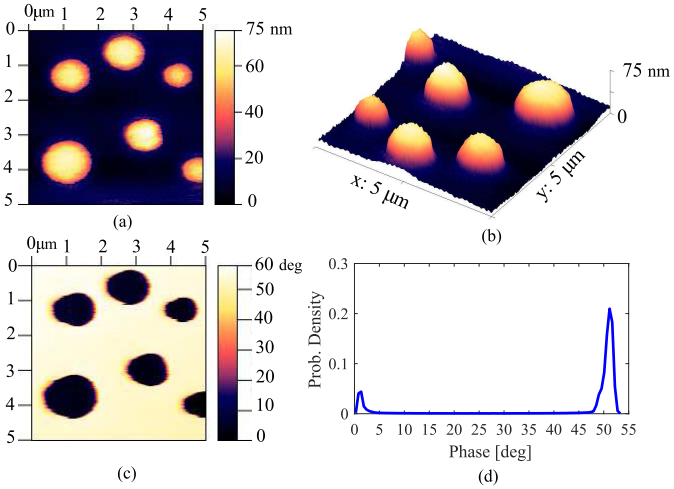

Fig. 10. Bimodal AFM imaging at the 1^{st} and 2^{nd} mode of the microcantilever on a LPDE sample: (a) 2D and (b) 3D topographic images at the 1^{st} mode. (c) Phase image at the 2^{nd} mode. (d) Histogram of the phase at the 2^{nd} mode.

V. Conclusion

We presented a new type of active microcantilever with a collocated sensor-actuator pair, which features a minimum feedthrough level to provide a high dynamic range and signal to noise ratio at 1^{st} and 2^{nd} resonance modes. These features make such cantilevers appropriate candidates for multifrequency AFM methods. To achieve a faster response time for operation at the 1^{st} mode, quality factor of the cantilever is actively modified. The positive position feedback *Q*-control technique is implemented by a modulated-demodulated approach. Tapping-mode AFM imaging experiments were conducted on a standard grating. While imaging at the 1^{st} mode, the results suggest that the *Q*-controlled cantilever provides a higher tracking bandwidth and consequently a higher z-axis controller gain to achieve a sharper transient response. Operating the cantilever at its 2^{nd} mode provides enough bandwidth for a fast response time without a applying a *Q*-controller. We also demonstrate application of the cantilever in a bimodal AFM imaging.

Disclaimer

Disclaimer: This report was prepared as an account of work sponsored by an agency of the United States Government. Neither the United States Government nor any agency thereof, nor any of their employees, makes any warranty, express or implied, or assumes any legal liability or responsibility for the accuracy, completeness, or usefulness of any information, apparatus, product, or process disclosed, or represents that its use would not infringe privately owned rights. Reference herein to any specific commercial product, process, or service by trade name, trademark, manufacturer, or otherwise does not necessarily constitute or imply its endorsement, recommendation, or favoring by the United States Government or any agency thereof. The views and opinions of authors expressed herein do not necessarily state or reflect those of the United States Government or any agency thereof.

References

[1] D. Sarid, T. G. Ruskell, R. K. Workman, and D. Chen, "Driven nonlinear atomic force microscopy cantilevers: From noncontact to tapping modes of operation," *J. Vac. Sci. Technol. B, Microelectron. Nanometer Struct.*, vol. 14, no. 2, pp. 864–867, 1996.

[2] T. Sulchek, G. G. Yaralioglu, C. F. Quate, and S. C. Minne, "Characterization and optimization of scan speed for tapping-mode atomic force microscopy," *Rev. Sci. Instrum.*, vol. 73, no. 8, pp. 2928–2936, Aug. 2002.

[3] J. D. Adams, L. Manning, B. Rogers, M. Jones, and S. C. Minne, "Self-sensing tapping mode atomic force microscopy," *Sens. Actuators A, Phys.*, vol. 121, no. 1, pp. 262–266, May 2005.

[4] M. B. Coskun, A. G. Fowler, M. Maroufi, and S. O. R. Moheimani, "On-chip feedthrough cancellation methods for microfabricated AFM cantilevers with integrated piezoelectric transducers," *J. Microelectromech. Syst.*, vol. 26, no. 6, pp. 1287–1297, Dec. 2017.

[5] M. B. Coskun, H. Alemansour, A. G. Fowler, M. Maroufi, and S. O. R. Moheimani, "*Q* control of an active AFM cantilever with differential sensing configuration," *IEEE Trans. Control Syst. Technol.*, vol. 27, no. 5, pp. 2271–2278, Sep. 2019.

[6] M. G. Ruppert and Y. K. Yong, "Note: Guaranteed collocated multimode control of an atomic force microscope cantilever using on-chip piezoelectric actuation and sensing," *Rev. Sci. Instrum.*, vol. 88, no. 8, Aug. 2017, Art. no. 086109.

[7] M. Mahdavi, M. B. Coskun, and S. O. R. Moheimani, "High dynamic range AFM cantilever with a collocated piezoelectric actuator-sensor pair," *J. Microelectromech. Syst.*, vol. 29, no. 2, pp. 260–267, Apr. 2020.

[8] I. R. Petersen and A. Lanzon, "Feedback control of negative-imaginary systems," *IEEE Control Syst.*, vol. 30, no. 5, pp. 54–72, Oct. 2010.

[9] K. Lau, D. E. Quevedo, B. J. G. Vautier, G. C. Goodwin, and S. O. R. Moheimani, "Design of modulated and demodulated controllers for flexible structures," *Control Eng. Pract.*, vol. 15, no. 3, pp. 377–388, Mar. 2007.

[10] K. S. Karvinen and S. O. R. Moheimani, "Modulated–demodulated control: Q control of an AFM microcantilever," *Mechatronics*, vol. 24, no. 6, pp. 661–671, Sep. 2014.

[11] R. Garcia and E. T. Herruzo, "The emergence of multifrequency force microscopy," *Nature Nanotechnol.*, vol. 7, no. 4, pp. 217–226, Apr. 2012.

[12] M. G. Ruppert, S. I. Moore, M. Zawierta, A. J. Fleming, G. Putrino, and Y. K. Yong, "Multimodal atomic force microscopy with optimized higher eigenmode sensitivity using on-chip piezoelectric actuation and sensing," *Nanotechnology*, vol. 30, no. 8, Jan. 2019, Art. no. 085503.

Mohammad Mahdavi (Member, IEEE) received the B.Sc. and M.Sc. degrees in electrical engineering from the University of Tehran, Tehran, Iran, in 2007 and 2010, respectively, and the Ph.D. degree in electrical engineering from The University of Texas at Dallas in May 2018. He is currently a Research Scientist with the Department of Systems Engineering, The University of Texas at Dallas. His main research interests involve design, microfabrication, and characterization of MEMS devices with special emphasis on resonant piezoelectric devices and high speed scanning probe microscopy.

Nastaran Nikooienejad received the B.Sc. degree in electrical engineering from Shiraz University, Shiraz, Iran, in 2006, and the M.Sc. degree in electrical engineering, as a distinguished student, from the Amirkabir University of Technology, Tehran, Iran, in 2009. She is currently pursuing the Ph.D. degree with the Department of Electrical and Computer Engineering, The University of Texas at Dallas, Richardson, TX, USA. Her research interests include control of MEMS devices, non-raster scanning methods, video-rate atomic force microscopy, and signal and image processing.

S. O. Reza Moheimani (Fellow, IEEE) currently holds the James Von Ehr Distinguished Chair in science and technology with the Department of Systems Engineering, The University of Texas at Dallas with appointments in the Electrical and Computer Engineering Department and the Mechanical Engineering Department. His current research interests include the applications of control and estimation in high-precision mechatronic systems, high-speed scanning probe microscopy and atomically precise manufacturing of solid-state quantum devices. He is a fellow of IFAC and the Institute of Physics, U.K. He was a recipient of several awards, including the IFAC Nathaniel B. Nichols Medal and the IEEE Control Systems Technology Award. He is an Editor-in-Chief of *Mechatronics*.